RESEARCH ARTICLE

CrossMark

Synthesis and characterization of anthill-eggshell composite adsorbent for removal of hexavalent chromium from aqueous solution

Adeyinka S. Yusuff[1] · Afeez O. Gbadamosi[2] · Mayowa A. Lala[1] · Jima F. Ngochindo[1]

Abstract

In this study, adsorption behavior of anthill-eggshell composite (AEC) for the removal of hexavalent chromium (Cr^{6+}) from aqueous solution was investigated. The raw AEC sample was thermally treated at 864 °C for 4 h and characterized using Brunauer-Emmett-Teller (BET), scanning electron microscopy (SEM), Fourier transform infrared (FTIR) spectroscopy, X-ray diffraction (XRD), and X-ray fluorescence (XRF) techniques. The effects of adsorption process variables including initial Cr^{6+} concentration, contact time, and adsorbent dosage on the Cr^{6+} removal efficiency were investigated using central composite design (CCD) of response surface methodology (RSM). Equilibrium adsorption isotherm and kinetic were also studied. From the analysis of variance (ANOVA), the three variables proved to be significant and the optimum conditions for Cr^{6+} adsorption were obtained to be 150 mg/L initial Cr^{6+} concentration, 45.04-min contact time, and 0.5 g adsorbent dosage, which resulted in 86.21% of Cr^{6+} adsorbed. Equilibrium isotherm study showed that Freundlich model fitted well to the experimental data. The pseudo-second-order kinetic model appeared to better describe the experimental data. The study showed that mixed anthill-eggshell is a promising adsorbent for removing Cr^{6+} from aqueous solution.

Keywords Adsorbent · Adsorption isotherm · Calcination · Equilibrium · Optimization

Introduction

The presence of pollutants such as organic and inorganic contaminants in water body is a result of population explosion and industrialization. However, domestic or industrial effluent needs to be treated before being released into water resources, because the presence of these contaminants at significant concentration is detrimental to both human and aquatic life. In particular, inorganic contaminant such as heavy metal renders serious havoc to humans as they are classified as one of the cancer-causing agents (Ridha et al. 2017). Heavy metals can easily penetrate into body tissues, thus leading to vital organs damage. For instance, chromium causes lung cancer,

gastrointestinal hemorrhage, acute renal failure, and pulmonary fibrosis (Ekanem 2017). Due to the risk associated with toxic heavy metals such as chromium, various tiers of government have mandated regulatory bodies to impose harsh and more stringent environmental laws on wastewater release. According to Nigeria Ministry of Environment, the maximum permitted level of chromium in water/wastewater is 0.01 mg/L. Meanwhile, the permissible concentration of chromium in wastewater, recommended by World Health Organization (WHO), is 0.05 mg/l (Wang and Lin 2008).

Several researchers have suggested various methods for removing dissolved toxic heavy metals from wastewater (Lim and Lee 2015; Ganesan et al. 2013; Vasudevan et al. 2011, 2013). Among the suggested techniques, adsorption of liquid/gas phase onto porous solid called adsorbent has been widely recommended. This is because, some of the adsorbents required for the separation of heavy metals from aqueous solution or natural wastewater can be cheaply synthesized from agricultural waste (Yusuff et al. 2017), industrial waste (Mohapatra et al. 2009), naturally occurring material (Mohamed et al. 2016), biomass (Ridha et al. 2017), and so on.

In recent time, research interest in low-cost, high adsorption capacity, non-toxic, thermally stable, and large surface

✉ Adeyinka S. Yusuff
  yusuffas@abuad.edu.ng

[1] Department of Chemical and Petroleum Engineering, College of Engineering, Afe Babalola University, Ado-Ekiti, Nigeria

[2] Faculty of Chemical and Energy Engineering, Universiti Teknologi Malaysia, 81310 Johor Bahru, Malaysia

🙋 Springer

area adsorbents, in particular, highly porous synthetic materials such as composite adsorbents derived from waste materials are still ongoing. Numerous researchers have synthesized composite adsorbents from different sources and applied them to remove heavy metals from aqueous environment (Yuan et al. 2009; Dousova et al. 2009). Khazaei et al. (2016) studied the adsorption capacity of partially reduced graphene oxide-Fe_3O_4 in removing lead ion from aqueous solution. Dousova et al. (2009) investigated the adsorption of Cr^{6+} from aqueous solution onto clay-iron oxide magnetic composites. A composite-derived nanoporous Ti-pillared montmorillonite adsorbent was synthesized by Na et al. (2010) for separating arsenic from synthetic solution. In this present study, however, a composite adsorbent was derived from anthill and chicken eggshell due to their ready availability. Eggshell is one of the household wastes (Yusuff et al. 2017). According to literature, typical dry eggshell contains more than 90% calcium carbonate (Sharma et al. 2010). It is thus possible to synthesize CaO-based adsorbent from eggshell due to high $CaCO_3$ content and intrinsic pore structure. Many studies on the use of eggshells as adsorbents to remove heavy metals and organic contaminants from aqueous environment have been reported (Eletta et al. 2016; Yusuff et al. 2017). However, the work conducted by Eletta et al. (2016) revealed that synthesized adsorbent from eggshell possesses one major adsorption site (CaO), which might not be sufficient enough to remove completely the adsorbate. The number of molecular adsorption sites could be enhanced by anchoring eggshell with another porous material such as anthill.

An anthill is a form of clay which is formed by workers ant. It is huge, surrounded by vegetation and can persist for several years. According to Akinwekomi et al. (2012), anthill sample is made up of silica (SiO_2), alumina (Al_2O_3), iron oxide (Fe_3O_4), and many other metal oxides. Numerous researchers have used SiO_2, Al_2O_3, and Fe_3O_4 as adsorbent ingredients/supports for heavy metal removal from aqueous solution. Fisli et al. (2017) employed $Fe_3O_4/SiO_2/TiO_2$ composite as adsorbent to remove contaminant from wastewater. Iron oxide (Fe_3O_4) supported on activated alumina (Al_2O_3) was used as adsorbent by Huang et al. (2000) for removing heavy metals from aqueous solution. Lim and Lee (2015) investigated the adsorption of Cu^{2+}, Zn^{2+}, and Pb^{2+} ions on soil containing oxides of silicon, aluminum, and iron. In the present work, a new composite material which was derived from anthill and chicken eggshell was used as a low-cost adsorbent for the removal of hexavalent chromium from aqueous solution and was characterized to gain insights into its physical, chemical, and morphological features. The effects of different variables, initial concentration, contact time, and adsorbent dosage, which affect the adsorption process, were investigated using central composite design (CCD) of response surface methodology (RSM). Moreover, the equilibrium adsorption isotherm and kinetic were studied in details.

Materials and methods

Materials

The waste chicken eggshells used in this study were collected from Afe Babalola University (ABUAD) farm, Ado-Ekiti, Nigeria, while anthill situated behind Fidelity Bank, ABUAD, Ado-Ekiti, Nigeria, was harvested. All the chemical compounds used in this study were of analytical grade (BDH, China) bought from Topyay Enterprise, Akure, Nigeria, and used as received without subjecting them to further purification. A stock solution (1000 mg/L) of Cr^{6+} was prepared by dissolving 2.83 g of potassium heptaoxodichromate (VI) [$K_2Cr_2O_7$] in 1 L of distilled water. From the 1 g/L of Cr^{6+} solution, 34.2, 50, 100, 150, and 165.8 mg/l were made by dilution method and subsequently used for batch adsorption experiment.

Preparation of anthill-eggshell composite adsorbent

The collected eggshell was soaked and thoroughly washed in tap water to remove dirt and white membrane. The neatly washed eggshells were then dried in an oven at 125 °C for 24 h in order to remove moisture content. The dried eggshells were later pulverized using mechanical grinder and obtained fine powder passed through sieve mesh of 0.3 mm to get very fine powder. The fine eggshell powder was kept in an enclosed plastic container. However, the harvested anthill was crushed by mortar and pestle and then sieved through 0.3 mm sieve mesh. The fine anthill powder obtained was kept in a plastic container.

The anthill-eggshell composite (AEC) was synthesized using optimum preparation conditions obtained from my previous study (Yusuff 2017). The anthill powder with a mixing ratio of 1: 1.86 on mass basis to the eggshell powder was dissolved in 125 mL of distilled water and stirred on a hot plate for 2 h to homogenize. The resulting mixture was thereafter dried in an oven overnight at 120 °C. Finally, the mixed anthill-eggshell was calcined in a muffle furnace at 864 °C for 4 h. The thermally treated AEC was poured in a beaker, covered and kept in a desiccator to prevent interference of atmospheric moisture and carbon dioxide (CO_2).

Characterization of AEC adsorbent

The physical and chemical properties of the as-synthesized AEC adsorbent were evaluated using Brunauer, Emmett, and Teller (BET) technique, scanning electron microscopy (SEM), Fourier transform infrared radiation (FTIR) spectroscopy, X-ray diffraction (XRD), and X-ray florescence (XRF). The textural characteristics of the AEC sample were determined by BET method using a Quantachrome instrument (Nova station A, version 11.03, USA) based on the

principle of adsorption/desorption of nitrogen at 77 K and 60/60 s (ads/des) equilibrium time. SEM (JEOL-JSM 7600F) examined the surface morphology of the prepared AEC adsorbent, while the surface functional groups on AEC adsorbent were determined by FTIR spectrophotometer (IR Affinity 1S, Shimadzu, Japan). XRD was used to confirm the structural characteristics and unique fingerprints of the AEC sample, which was conducted on a model Rigaku D/Max-IIIC XRD (PW 1800) analyzer. A Cu kα radiation (1.556 Å) was employed to generate diffraction patterns at ambient temperature in the scanning angle 2θ of 5–90°. XRF analysis was carried out using a skyray simultaneous ED-XRF analyzer model EOX3600B to determine the chemical compositions of the prepared AEC adsorbent.

Experimental design

Response surface methodology (RSM) is a combination of mathematical and statistical optimization tools that are often used to correlate the relationship between output and input variables (Tan et al. 2008). It involves the use of design expert software that can be employed to estimate the interaction between controlled experimental variables and measured response (Muthu and Viruthagiri 2015). In addition, it assists in designing the best experimental procedures in order to evaluate or assess the interrelationship among the experimental variables. In this study, central composite design (CCD), one of the several methods of optimization embedded in RSM, was employed to study the influence of variables on Cr^{6+} adsorption. CCD is a suitable technique usually employed in designing the experimental procedures in order to acquire necessary information for examining lack of fit without necessarily considering numerous design points (Montgomery 2005). In addition, it is a powerful tool for evaluating the output parameter(s) of most of the steady-state processes (Obeng et al. 2005). There are three portions in CCD implementation, namely, a composite or partial 2^k factorial design whose factor levels are coded as − 1, 1 called factorial portion, an axial portion consisting of 2 k points (Khuri and Mukhopadhyay 2010) and center point (n$_o$).

In the present work, adsorption of Cr^{6+} on as-synthesized AEC adsorbent was conducted under batch operation and process variables which include initial Cr^{6+} concentration, C, contact time, t, and adsorbent dosage, d, were varied using the CCD. Table 1 presents five level-three factor CCD for

the Cr^{6+} removal from aqueous solution by AEC via batch mode adsorption.

The main objective is to determine optimum values of process parameters that would provide maximum Cr^{6+} removal efficiency. However, the response was determined via adsorption process and also used to develop a mathematical model, which correlate the removal efficiency, R (%) to those three independent variables considered through first order, second order and interaction terms, according to the Eq. 1.

$$R = a_0 + a_1C + a_2t + a_3d + a_{12}Ct + a_{13}Cd + a_{23}td$$
$$+ a_{11}C^2 + a_{22}t^2 + a_{33}d^2 \qquad (1)$$

where R is the response variable of Cr^{6+} removal efficiency. The a_{is} are regression coefficients for linear effects; a_{ik} the regression coefficients for quadratic effects and C, t and d represent coded experimental level of the variables.

Batch adsorption experiment

Batch adsorption study was conducted by bringing into contact the prepared AEC adsorbent with solution of Cr^{6+} in a set of each 250-mL conical flasks. The flasks were covered and shaken in a temperature controlled water bath shaker (SearchTech Instrument) operating at a constant stirring speed of 150 rpm. The process was carried out by considering the following adsorption conditions: initial Cr^{6+} concentration (50–150 mg/L), contact time (30–120 min), and adsorbent dosage (0.5–2.5 g) at pH of 4.5 and constant room temperature of 27 ± 1 °C. Upon equilibrium attainment, each sample was centrifuged at high speed for 10 min and decanted. The concentration of un-adsorbed Cr^{6+} was then determined by Atomic Absorption Spectrophotometer (AAS, Buck Scientific 210VGP, USA). The Cr^{6+} removal efficiency, R (%), and equilibrium amount of Cr^{6+} adsorbed, q_e, mg/g, were calculated by Eqs. (2) and (3) as follows.

$$R, \% = \frac{(C_o - C_e) \, x \, 100\%}{C_o} \qquad (2)$$

$$q_e = \frac{(C_o - C_e)V}{M} \qquad (3)$$

where C_o and C_e (mg/L) are the initial and equilibrium concentration of Cr^{6+} in aqueous phase. V (L) is the volume of the Cr^{6+} solution, and M (g) is the mass of AEC adsorbent used.

Table 1 Studied range of each variable in actual and coded form

Variable	Unit	Low level (− 1)	Center point (0)	High level (+ 1)
Initial Cr^{6+} concentration (C)	mg/L	50	100	150
Contact time (t)	min	30	75	120
Adsorbent dosage (d)	g	0.5	1.5	2.5

Equilibrium adsorption isotherm

Two parameters isotherm models, namely, Langmuir and Freundlich, were used to evaluate the experimental data. The Langmuir and Freundlich isotherm models are given in Eqs. (4) and (5) respectively as follows:

$$q_e = \frac{q_{\max} bC_e}{(1 + bC_e)} \qquad (4)$$

$$q_e = k_F C_e^{1/n} \qquad (5)$$

where q_e(mg/g) is the amount of metal ions adsorbed at equilibrium, C_e(mg/L) is the equilibrium concentration of metal in solution, $q_{\max}$(mg/g) is the maximum adsorption capacity, b is the Langmuir equilibrium constant, k_F (mg/g(L/mg)$^{1/n}$) indicates the adsorption capacity of the adsorbent, and n is an adsorption intensity.

A dimensionless constant referred to as separation factor (R_L) is applied to ascertain the nature of adsorption by using the Langmuir equilibrium constant (b) and the highest initial concentration of Cr^{6+} (C_o, mg/L) as given in Eq. (6).

$$R_L = \frac{1}{(1 + bC_O)} \qquad (6)$$

Separation factor (R_L) can either indicate irreversible adsorption ($R_L = 0$), favorable adsorption ($0 < R_L < 1$), linear adsorption ($R_L = 1$) or unfavorable adsorption ($R_L > 1$).

Adsorption kinetics

In this study, two different kinetic models, namely pseudo-second-order and pseudo-second-order models were applied to evaluate the experimental data obtained in order to establish the kinetics of hexavalent chromium adsorption onto anthill-eggshell composite.

Pseudo-first-order model

The pseudo-first-order kinetic model is often used to describe the adsorption of adsorbate from a solution onto porous solid material. The pseudo-first-order Lagregren model is generally expressed as follows (Ganesan et al. 2013):

$$dq_t/dt = k_1(q_e - q_t) \qquad (7)$$

where q_e (mg/g) is the amount of Cr^{6+} adsorbed at equilibrium, q_t is the amount of Cr^{6+} adsorbed at time t (mg/g), and k_1 is the pseudo-first-order rate (min^{-1}). The integration of Eq. (7) with the boundary conditions $q_e = 0$ at $t = 0$ and $q_e > 0$ at $t > 0$ yielded Eq. (8).

$$\log(q_e - q_t) = \log q_e - \frac{k_1 t}{2.303} \qquad (8)$$

Pseudo-second-order model

The pseudo-second-order kinetic model according to Ho and McKay (1998) is expressed as:

$$dq_t/dt = k_2(q_e - q_t)^2 \qquad (9)$$

where q_e (mg/g) is the amount of Cr^{6+} adsorbed at equilibrium, q_t is the amount of Cr^{6+} adsorbed at time t (mg/g), and k_2 is the pseudo-second-order (g mg^{-1} min^{-1}). The integration of Eq. (9) with the boundary conditions $q_e = 0$ at $t = 0$ and $q_e > 0$ at $t > 0$ and after much algebraic manipulation is obtained to be:

$$\frac{t}{q_t} = \frac{1}{k_2 q_e^2} + \frac{t}{q_e} \qquad (10)$$

In order to further examine the applicability of the pseudo-second-order kinetic model, the initial sorption rate h (mg/g min) as time (t) approaches zero was determined as follows:

$$h = k_2 q_e^2 \qquad (11)$$

Results and discussions

Characterization of AEC adsorbent

BET analysis

The results of textural feature analysis are presented in Table 2, it was observed that the thermally treated AEC possessed high surface area when compared to the surface areas of thermally activated chicken eggshell and clay, which were reported to be 54.6 and 34.61 m^2/g by Tan et al. (2015) and Olutoye and Hameed (2013) respectively. In addition, the average pore diameter of AEC was also found to be large especially when compared with microfibrous chitosan-sepiolite nanocomposite (Darder et al. 2006) and montmorillonite-supported magnetite nanocomposite (Yuan et al. 2009). This result indicates that there are numerous molecular adsorption sites on AEC surface and they can enhance adsorption due to larger pore diameter thus better possibility for Cr^{6+} to be adsorbed.

SEM analysis

The SEM image of AEC adsorbent before and after Cr^{6+} adsorption was presented in Fig. 1. It was evidently clear that

Table 2 Textural characteristic of as-synthesized AEC adsorbent

| Parameter	Value
BET surface area (m^2/g)	91.08
Total pore volume (cm^3/g)	0.2007
Average pore diameter (Å)	36.75

Fig. 1 SEM images of AEC adsorbent **a** before adsorption and **b** after adsorption

(a)   (b)
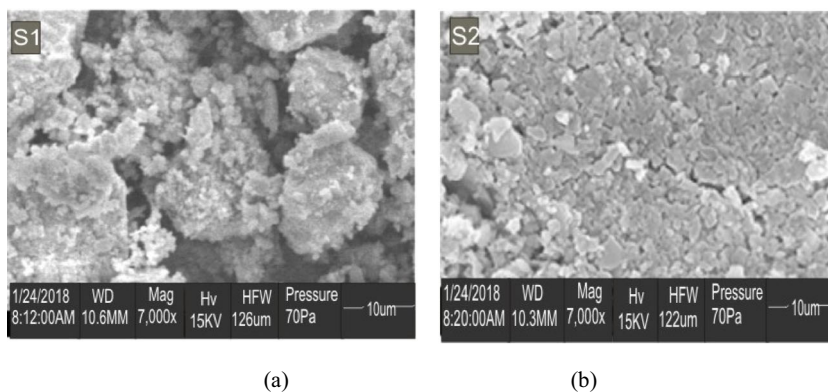
there were various pores on the surface of fresh AEC sample as can be seen in Fig. 1a, indicative of better possibility for Cr^{6+} to be attached to its surface. The pores observed on the thermally activated AEC was a result of complete removal of adsorbed gases and organic matter, thus transforming the components into mixed metal oxides (Olutoye and Hameed 2013). This is substantiated by the results of XRD and XRF analyses and is the main reason why AEC exhibited better performance in removing Cr^{6+} from aqueous solution. Meanwhile, virtually, all the pores were blocked due to Cr^{6+} adsorption onto AEC adsorbent as shown in Fig. 1b.

FTIR analysis

The FTIR spectra of raw, calcined, and used AEC adsorbents are presented in Fig. 2. The sharp absorption peak at 3640 cm^{-1} in both calcined and used AEC and broad bands 3400 cm^{-1} for the three samples are attributed to O-H stretching vibration mode from Si-Si-OH or Al-Al-OH, indicative of moisture on the adsorbent surface (Fisli et al. 2007). The absorption bands 2870 and 2513 cm^{-1} for raw, calcined, and used AEC samples are assignable to the C-H symmetric stretching and C–H bonds in the methylene groups respectively. A similar peak 2360 cm^{-1} observed in both raw and used AEC samples corresponded to C=N stretching. The absorption peaks at 1797 cm^{-1} for the three samples can be attributed
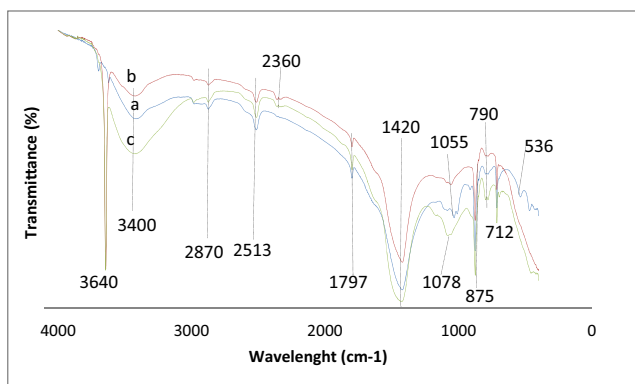
to C=O stretching of aldehydes. The observed peaks at 1420, 875, and 712 cm^{-1} in all the samples are attributed to C-O asymmetric stretching, out of plane bend, and in-plane bend vibration modes respectively, while the presence of peaks at 1055 cm^{-1} in both raw and calcined samples are attributed to Al-Al-OH clay vibration. The band at 1078 cm^{-1} for used AEC samples is attributed to Si-O-Si stretching. As well the observed band at 536 cm^{-1} in raw AEC was due to the Al-OH stretching vibration (Olutoye and Hameed 2013). The presence of these functional groups contributes to the better performance of AEC adsorbent.

XRD analysis

The result of XRD analysis conducted on AEC adsorbent is shown in Fig. 3; it can be observed clearly that the thermally treated adsorbent comprised of calcium oxide (CaO), silica (SiO_2), Al (silicate) [mixture of Al_2O_3 and SiO_2], illite and kaolinite ($Al_2O_3.2SiO_2.2H_2O$) phases. However, CaO, SiO_2, and Al (silicate) were the major phases. This observation implies that there was complete decomposition of $CaCO_3$ contained in the eggshell into CaO and CO_2 as there is no trace of $CaCO_3$ in the XRD pattern. More so, upon calcination, the anthill transformed into phases of mixed metal oxides as can be seen in Fig. 3. It is observed that the major peaks occurred at 2θ equal to 6.18°, 15.64°, 44.35°, 54.13°, 65.22°, and 80.55° were attributed to CaO, while peaks at 2θ equal to 20.17°, 22.22°, 40.34°, 55.22°, and 75.20° corresponded to SiO_2 phase. Al(silicate) occurred at 2θ equal to 10.57°, 25.35°, 34.9°, and 69.49°. The minor kaolinite peak was observed at 2θ equal to 85.33°. The XRD result shown in Fig. 3 revealed that the silicon and aluminum exist in conjunction with magnesium, iron, and potassium oxides in the form of illite [$(K, H_3O) (Al, Mg, Fe)_2 (Si, Al)_4O_{10}$] at 2θ equal to 35.02° of the XRD spectra shown in Fig. 3. This is corroborated by the FTIR and XRF analyses. A similar observation was reported by Olutoye and Hameed (2013). However, having discovered that AEC adsorbent contained SiO_2, Al_2O_3, and other metal oxides, there is good possibility for maximum Cr^{6+} uptake from aqueous solution to be removed. This is

Fig. 2 FTIR spectra of (a) raw, (b) calcined, and (c) used AEC adsorbents

Fig. 3 XRD spectra of thermally treated AEC adsorbent
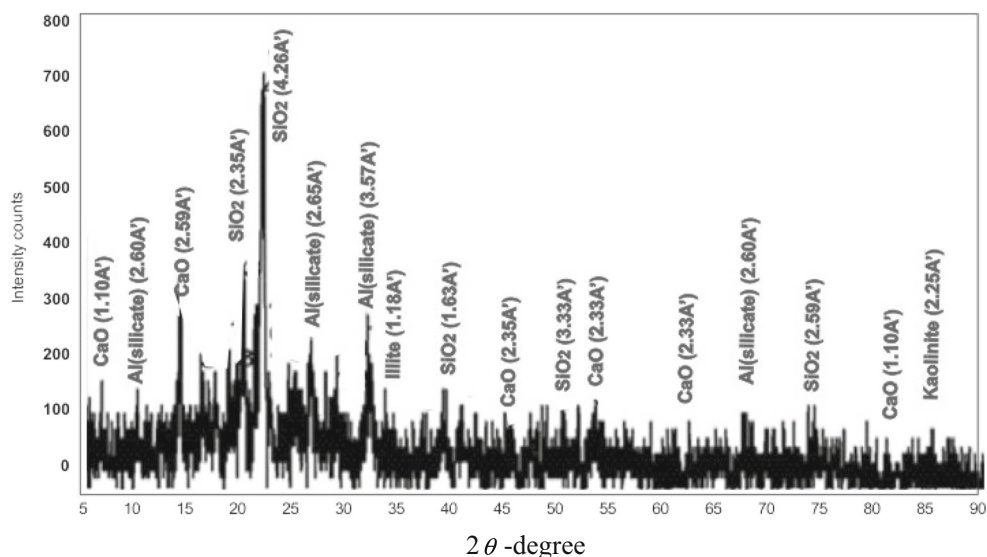
because there is electrostatic interaction of the adsorbate with surface silica and alumina sites (Mohapatra et al. 2009).

XRF analysis

The mineral composition of raw and calcined AEC adsorbents is presented in Table 3. It could be deduced from the XRF analysis that there was increased in CaO content after calcination of raw AEC. This observation is attributed to liberation of CO_2 and other adsorbed gases at higher calcination temperature. A similar observation was reported by Tan et al. (2015). Meanwhile, there was decreased in SiO_2, Al_2O_3, Fe_2O_3, and others, while Na_2O and K_2O were not detected after calcination of raw adsorbent. The drop in weight compositions of these metal oxides is attributed to removal of some bound hydroxyl groups and liberation of adsorbed gases from the thermally treated AEC which created cavities on the adsorbent surface for improved adsorption of Cr^{6+} from aqueous solution. This fact can be corroborated by the SEM, FTIR and XRD results and is attributed to why high loss of ignition (LOI) was recorded after calcination, as depicted in Table 3.

In this present study, it was noticed that calcination at 864 °C for 4 h was able to transform raw AEC into a synergetic mixed oxide structure. Thus, the reported literature and the result obtained herein imply that not only CaO plays a role in the adsorbent performance, but also the other oxides contained in the treated sample can determine the form of molecular adsorption sites and their level of capacity.

Regression model development

The result presented in Table 4 is the batch mode adsorption process variables in both coded and actual values together with their corresponding measured responses (Cr^{6+} removal efficiencies). Based on CCD, a quadratic model given in Eq.

(7) was developed to correlate the input variables to the response.

$$R = 71.06 + 2.47C - 5.24t$$
$$+ 1.99d - 3.12Ct - 7.05Cd - 3.80td$$
$$+ 0.71C^2 - 0.85t^2 + 0.21d^2 \qquad (7)$$

In the present study, linear correlation coefficient (R^2) was used as criteria to test for the fitness of the developed model. The principle is that the closer the R^2 value to unity the more accurate the Cr^{6+} adsorbed response could be predicted by the model (Yusuff 2017). The R^2 value for the developed model is 0.9586 and this implied that 95.86% of total variation in the adsorption of Cr^{6+} on AEC adsorbent is attributed to experimental parameters considered in the present study. However, the high R^2 value obtained is an indication that there was mutual agreement between predicted and experimental values of Cr^{6+} uptake as can also be seen in Table 4.

Table 3 XRF results for the raw and calcined AEC adsorbents

Chemical composition (wt%)	Raw	Calcined
Al_2O_3	4.95	1.26
SiO_2	14.03	8.63
Na_2O	0.01	–
SO_3	0.98	0.62
K_2O	0.04	–
CaO	78.52	84.92
Fe_2O_3	2.58	2.28
MgO	0.64	0.69
TiO_2	0.67	0.42
LOI	5.68	8.01

Table 4 Batch mode adsorption process parameters in coded and actual values with Cr^{6+} removal efficiencies (responses) from experimental results

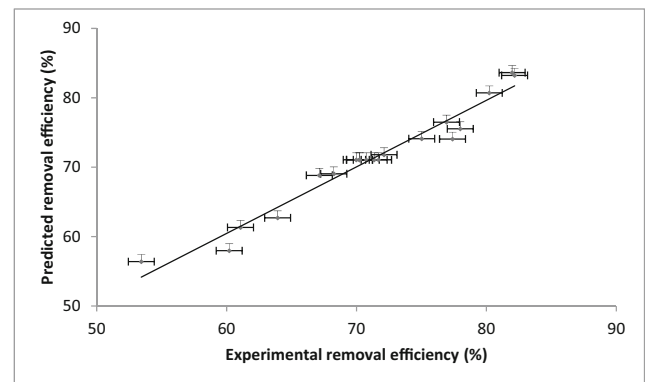| Run no.	Levels			Batch adsorption process variables			Cr^{6+} removal efficiency, R (%)	
				Initial Cr^{6+} concentration, C (mg/L)	Contact time, t (min)	Adsorbent dosage, d (g)	Predicted value	Experimental value
1	−1	−1	−1	50	30	0.5	57.96	60.20
2	+1	−1	−1	150	30	0.5	83.22	82.17
3	−1	+1	−1	50	120	0.5	61.31	61.07
4	+1	+1	−1	150	120	0.5	74.10	75.02
5	−1	−1	+1	50	30	2.5	83.62	81.98
6	+1	−1	+1	150	30	2.5	80.70	80.22
7	−1	+1	+1	50	120	2.5	71.79	72.12
8	+1	+1	+1	150	120	2.5	56.39	53.43
9	−α	0	0	34.2	75	1.5	69.04	68.25
10	+α	0	0	165.8	75	1.5	75.53	77.99
11	0	-α	0	100	15.78	1.5	76.49	76.93
12	0	+α	0	100	134.22	1.5	62.70	63.93
13	0	0	-α	100	75	0.18	68.82	67.14
14	0	0	+α	100	75	2.82	74.04	77.39
15	0	0	0	100	75	1.5	71.36	71.06
16	0	0	0	100	75	1.5	70.24	71.06
17	0	0	0	100	75	1.5	69.98	71.06
18	0	0	0	100	75	1.5	71.70	71.06
19	0	0	0	100	75	1.5	70.22	71.06
20	0	0	0`	100	75	1.5	70.75	71.06

With the use of analysis of variance (ANOVA), the adequacy of the developed model was further evaluated and the results according to ANOVA are presented in Table 5. The model was significant with the probability of error value (P value) less than 0.0001 to predict the values of removal efficiencies. In addition, the model F value which was obtained to be 25.76 reaffirmed the model significance. When value of prob. > F is less 0.05, it indicates that the model terms are significant. In this regards, however, C, t, d, Ct, Cd, and td were significant model terms, while all the quadratic model terms, C^2, t^2, and d^2 were all insignificant to the predicted Cr^{6+} removal efficiency. Nevertheless, as can be seen in Table 5, it was evidently clear that the developed model was appropriate to predict Cr^{6+} removal efficiency within the range of parameters studied.

The plot of predicted Cr^{6+} uptake against the experimental Cr^{6+} uptake was depicted in Fig. 4. In the plot, it was observed that the values of predicted removal efficiency were quite

Table 5 ANOVA table for the model and the model terms

Source	F value	Prob. > F
Model	25.76	< 0.0001 significant
C-Initial Cr^{6+} concentration	15.75	0.0026
t-Contact time	70.95	< 0.0001
d-Adsorbent dosage	10.21	0.0096
Ct	17.56	0.0019
Cd	89.63	< 0.0001
td	26.01	0.0005
C^2	0.79	0.3957
t^2	1.12	0.3141
d^2	0.072	0.7938
R^2 value	–	0.9586
Adj. R^2	–	0.9214
Pred. R^2	–	0.6402

Fig. 4 Predicted vs. experimental Cr^{6+} removal efficiency

(a)

(b)

(c)
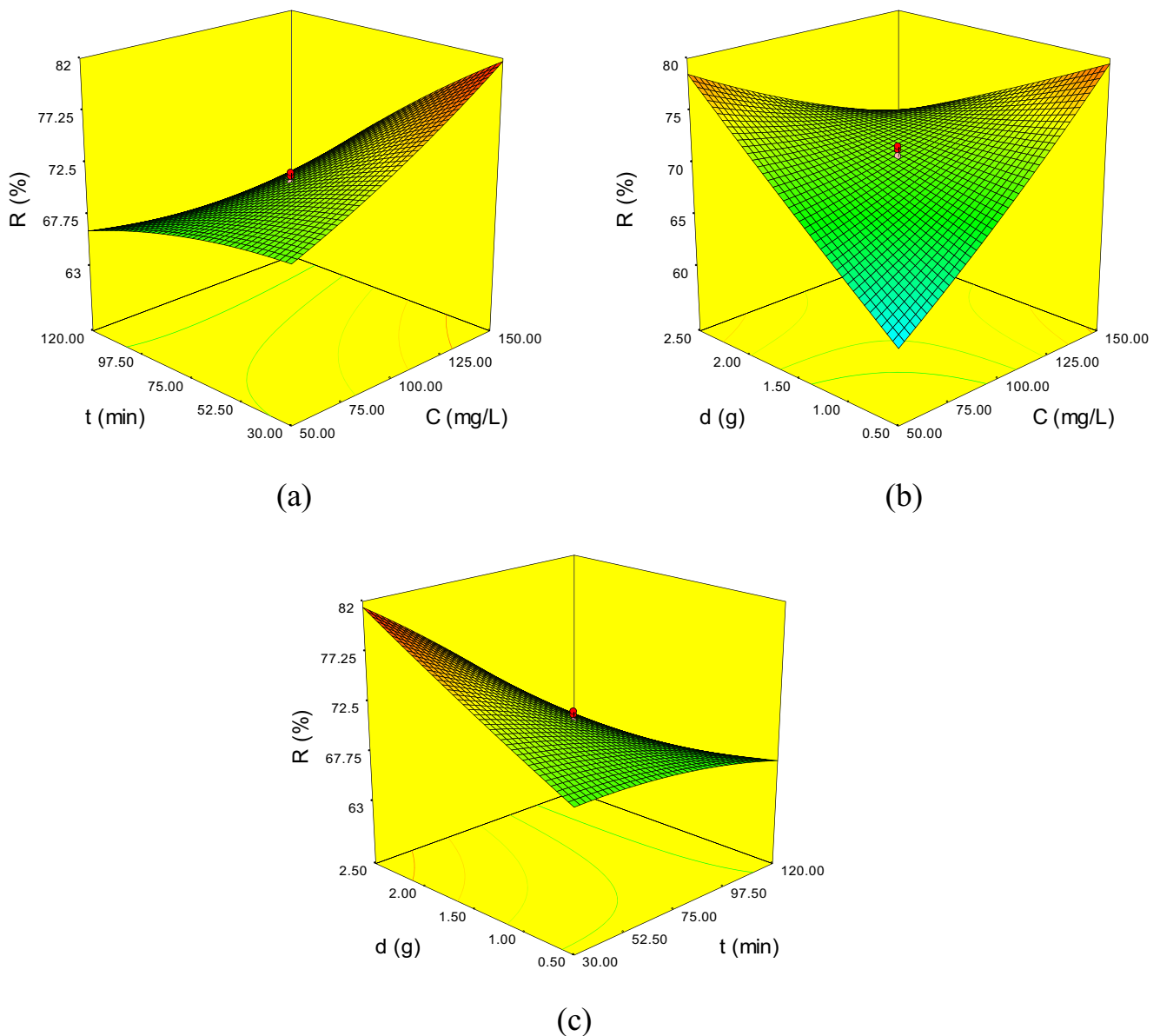
Fig. 5 Interactive effect of parameters on the removal efficiency of Cr^{6+} **a** concentration vs. contact time, **b** concentration vs. adsorbent dosage, and **c** adsorbent dosage vs. contact time

intimate to the actual values of removal efficiency, which indicates smaller error between the two responses. This observation was corroborated by the R^2 value of the model, as explained earlier.

Effect of adsorption process variables

As revealed by analysis of variance (ANOVA), the three process variables studied have significant effects on Cr^{6+} uptake. More so, the effect of various interactions between the process variables proved to be significant. This research output revealed the beauty of using design of experiment in examining the interaction among variables that influence the adsorption of Cr^{6+} on AEC adsorbent. The significant influences of the
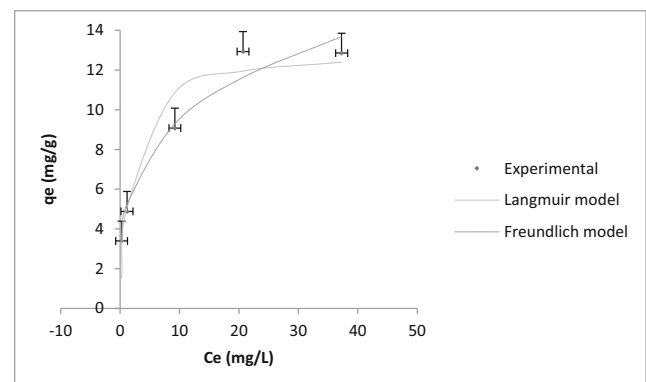
Fig. 6 Two-parameter isotherm models for adsorption of Cr^{6+} onto AEC at contact time = 45.04 min and adsorbent dosage = 0.5 g

Table 6 Two-parameter isotherm constants and correlation coefficients for adsorption of Cr^{6+} onto AEC adsorbent

Isotherm	Value
Langmuir	
q_{max} (mg/g)	12.99
b (L/mg)	0.555
R^2	0.9209
R_L	0.012
Freundlich	
k_F (mg/g(L/mg)$^{1/n}$)	5.03
n (mg/g)	3.62
R^2	0.9673

initial Cr^{6+} concentration, contact time, and adsorbent dosage on the removal efficiency of Cr^{6+} are attributed to their F values (Table 5). In the present study, contact time is more relevant to hexavalent chromium removal from aqueous solution compared to concentration and adsorbent dosage as confirmed by its F value in the ANOVA (Table 5).

The three-dimensional plots for the three parameters studied are presented in Fig. 5. The interactive effect of initial Cr^{6+} concentration, C, and contact time, t, is presented in Fig. 5a. It was observed that for almost 82% Cr^{6+} uptake, initial concentration of 150 mg/L would be treated for 30 min. This implied that for initial Cr^{6+} concentration of 150 mg/L used there was a rapid removal of the adsorbate from aqueous solution during 30 min of the operation. The reason is due to availability of more than enough surface adsorption sites of AEC for the increasing initial concentration. The same trend of observation was reported by Vasudevan and Lakshmi (2012).

The combined effect of initial Cr^{6+} concentration and AEC dosage which is shown in Fig. 5b referred to a removal efficiency of around 80% for 50 mg/L initial Cr^{6+} concentration which was treated with 2.5 g AEC. This observation is attributed to large dose of AEC used which contains several active adsorptive sites for the increasing initial Cr^{6+} concentration. A similar observation was reported by Malkoc (2006). Depicted in Fig. 5c is the interactive effect of contact time and AEC

dosage which gave a maximum Cr^{6+} removal efficiency of 81.55% at 2.5 g AEC dose for 30-min contact time.

The optimum Cr^{6+} removal efficiency was determined considering adsorption process condition as 150 mg/L initial adsorbate concentration, 45.04 min contact time and 0.5 g AEC dosage, which resulted in 86.21% Cr^{6+} uptake from aqueous solution. However, the predicted removal efficiency of Cr^{6+} according to CCD was suggested to be 82.17%. It was therefore noted that there was good agreement between experimental and predicted Cr^{6+} removal efficiency, with relatively error of 4.69%.

Equilibrium isotherm studies

In testing the applicability of Langmuir and Freundlich isotherms, the Cr^{6+} initial concentration employed was from 34.2 to 165.8 mg/L. For both isotherms, the experimental data are plotted as q_e against C_e by non-linear Eqs. (4) and (5). From Fig. 6 which depicts a comparison of the experimental data with the Langmuir and Freundlich isotherms, the values of the parameters contained in the two isotherm models were determined and presented in Table 6. However, the applicability of the two isotherms considered was compared using linear correlation coefficient (R^2). The values of R^2 for both isotherms were also presented in Table 6. Based on the values of R^2, Freundlich isotherm provides the best fit to the adsorption equilibrium data of Cr^{6+}. This indicates that the adsorption of Cr^{6+} by AEC adsorbent is evidently with multilayer and heterogeneous adsorption sites. A similar observation was reported for adsorption of Cr^{6+} from aqueous solution by natural clinoptilolite zeolite (Jorfi et al. 2017). As can be seen in Table 6 as well, the value of separation factor (R_L) obtained for Cr^{6+} was less than one, indicative of favorable adsorption operation, and Langmuir constant (b) which is attributed to the affinity between adsorbate and adsorbent was found to be 0.555. The value of Freundlich exponent n (3.62) was found to be lied between 0 and 10. Thus, this indicates that the adsorption of Cr^{6+} ions onto AEC was favorable (Vasudevan and Lakshmi 2012; Ganesan et al. 2013).

Table 7 Comparison of maximum adsorption capacities of different adsorbents for Cr^{6+} removal from aqueous system

Adsorbent	Maximum adsorption capacity (mg/g)	Reference
Distillery sludge	5.7	Selvaraj et al. (2003)
Montmorillonite-supported magnetite nanoparticle	15.3	Yuan et al. (2009)
Peanut shell	8.31	Al-Othman et al. (2012)
Natural clinoptilonite zeolite	10.42	Jorfi et al. (2017)
Australian zeolite	5–11.2	Nguyen et al. (2015)
Mango kernel	7.8	Rai et al. (2016)
Maple sawdust	5.1	Yu et al. (2003)
Teak sawdust	0.89	Sumathi et al. (2005)
Anthill-eggshell composite (AEC)	12.99	Current study
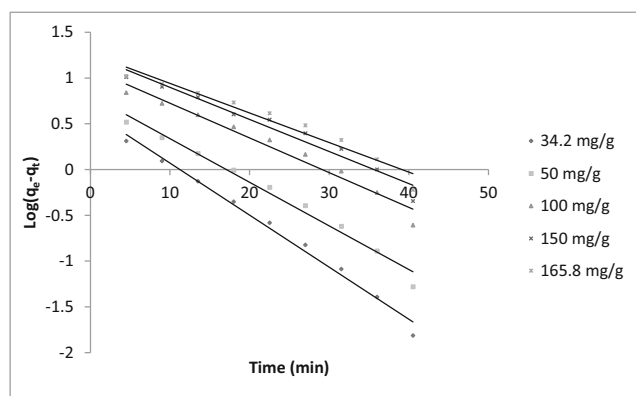
Fig. 7 Pseudo-first-order kinetics for adsorption of Cr^{6+} on AEC
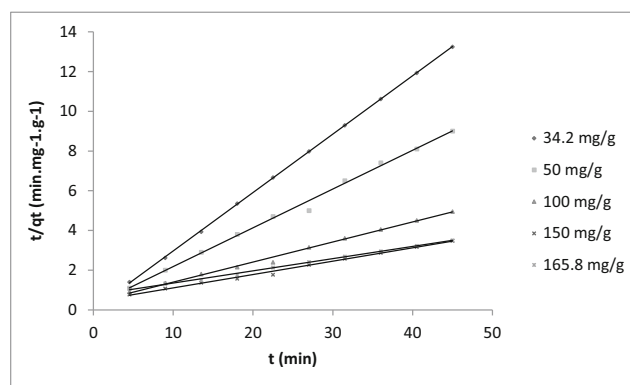

Fig. 8 Pseudo-second-order kinetics for adsorption of Cr^{6+} on AEC

In addition, comparing the maximum adsorption capacity (q_{max}) of different adsorbents for Cr^{6+} removal from aqueous solutions as shown in Table 7, AEC is found to possess a maximum adsorption capacity of 12.99 mg/g at room temperature and this implies that AEC could be regarded as an effective adsorbent for the removal of Cr^{6+} from wastewater/aqueous solution, especially when compared with peanut shell (8.31 mg/g, Al-Othman et al. 2012) and natural clinoptilolite zeolite (10.42 mg/g, Jorfi et al. 2017).

Adsorption kinetics

The change in amount of Cr^{6+} adsorbed with time was kinetically analyzed using pseudo-first-order and pseudo-second-order models. The parameters contained in pseudo-first-order model (q_e and k_1) and linear correlation coefficients for all initial Cr^{6+} concentrations considered in this study were determined from the plot of $\log(q_e - q_t)$ against t as shown in Fig. 7 and the values obtained are presented in Table 8. The results revealed that the calculated values of q_e did not conform with the experimental values of q_e at all initial Cr^{6+} concentrations studied with R^2 values generally less than 0.990. This indicates that the adsorption of Cr^{6+} on AEC could not be described by the pseudo-first-order kinetic. Similar observations were also reported by Vasudevan and Lakshimi (2012) and Kamaraj et al. (2015). Therefore, the experimental data were further examined using pseudo-second-order kinetic model.

The pseudo-second-order kinetic model parameters (q_e and k_2) and linear correlation coefficients (R^2) for all the initial Cr^{6+} concentrations were determined from the plot of t/q_t against t (Fig. 8) and their values are presented in Table 8 as well. The plots were observed to be linear with R^2 values for all the initial concentrations very close to unity. This observation implies that the possibility of the chemisorption playing a significant role in the rate-determining step cannot be neglected (Lim and Lee 2015). As can be seen in Table 8, the calculated values of q_e agreed reasonably well with the experimental q_e values at all initial Cr^{6+} concentrations considered. This indicates that the experimental data fitted very well the pseudo-second-order kinetic model and can be employed to favorably describe the adsorption of Cr^{6+} onto AEC.

Table 8 shows the results obtained from the pseudo-first-order and pseudo-second-order kinetic models. It was found that the correlation coefficients for the pseudo-second-order model were relatively greater than those obtained for the pseudo-first-order model for the five different initial Cr^{6+} concentrations considered. The obtained results showed that the adsorption of Cr^{6+} onto AEC could best be described and predicted by the pseudo-second-order kinetic model. The maximum initial sorption rate (h) of 1.181 mg/g min was obtained at the initial Cr^{6+} concentration of 100 mg/g as can be seen in Table 8 as well. This observation is probably attributed to the increase in the driving force for mass transfer,

Table 8 Kinetic models and parameters of adsorption of Cr^{6+} onto AEC

C_o (mg/L)	Pseudo-first-order				Pseudo-second-order			
	$q_{e, exp}$ (mg/g)	$q_{e, cal}$ (mg/g)	k_1 (min^{-1})	R^2	$q_{e, cal}$ (mg/g)	k_2 (g/mg min)	R^2	h (mg/g min)
34.2	3.396	1.895	0.131	0.9892	3.401	0.086	0.9999	0.995
50	4.885	2.259	0.110	0.9817	5.131	0.038	0.9954	1.000
100	9.079	3.015	0.087	0.9664	9.921	0.012	0.9951	1.181
150	12.93	3.485	0.081	0.9609	14.86	0.005	0.9947	1.104
165.8	12.85	3.541	0.074	0.9509	16.29	0.004	0.9978	1.061

which allows rapid movement of Cr^{6+} ions to the surface of the adsorbent (Hameed et al. 2009).

Conclusion

This finding revealed the potential of anthill-eggshell composite as an effective adsorbent for the removal of Cr^{6+} from aqueous solution. The characterization results showed that AEC possessed CaO, SiO_2, Al_2O_3, and Fe_2O_3 as its major adsorption sites. The optimal condition obtained for the Cr^{6+}/AEC system was initial adsorbate concentration of 150 mg/L, contact time of 45.04 min, and AEC dosage of 0.5 g. The optimized condition was validated with the true Cr^{6+} removal efficiency of 86.21%. Experimental data acquired agreed excellently well with Freundlich isotherm model. The value of the Freundlich exponent (n) was greater than one, implied the adsorption of Cr^{6+} on AEC was a favorable operation. This batch mode adsorption operation which focused on removal of Cr^{6+} from synthetic solution resulted in meaningful outcome, and it is our wish to determine the exact adsorption capacity of AEC as an adsorbent by using it for the removal of heavy metals from industrial effluents and the results obtained in the present study indicated that AEC is a potential composite adsorbent capable of removing dissolved toxic heavy metals from natural wastewater.

References

Akinwekomi AD, Omotoyinbo JA, Folorunso D (2012) Effect of high alumina cement on selected foundry properties of anthill clay. Leonardo Electron J Pract Technol 1:37–46

Al-Othman Z, Ali R, Naushat M (2012) Hexavalent chromium removal from aqueous medium by activated carbon prepared from peanut shell: adsorption kinetics, equilibrium and thermodynamic studies. Chem Eng J 184:238–247

Darder M, López-Blanco M, Aranda P, Aznar AJ, Bravo J, Ruiz-Hitzky E (2006) Microfibrous chitosan—sepiolite nanocomposites. Chem Mater 18:1602–1610

Dousova B, Grygar T, Martaus T, Kolousek D, Machovic V (2009) Characterization of Fe-treated clays as effective adsorbent for Cr^{6+} removal from aqueous solution. J Hazard Mater 165:134–140

Ekanem SE (2017) Adsorption of copper ion from aqueous solution onto thermally treated eggshell: kinetic and equilibrium study. B. Eng Thesis, Department of Chemical & Petroleum Engineering, Afe Babalola University, Ado-Ekiti, Nigeria

Eletta OAA, Ajayi OA, Ogunleye OO, Akpan IC (2016) Adsorption of cyanide from aqueous solution using calcinated eggshells: equilibrium and optimization studies. J Environ Chem Eng 4:1367–1375

Fisli A, Krisnanandi YK, Gunlazuardi J (2017) Preparation and characterization of Fe_2O_3/SiO_2/TiO_2 composite for methylene blue removal in water. Int J Technol 1:76–84

Ganesan P, Kamaraj R, Sozhan G, Vasudevan S (2013) Oxidized multi walled carbon nanotube as adsorbent for the removal of manganese from aqueous solution. Environ Sci Pollut Res 20:987–996

Hameed BH, Krishni RR, Sata SA (2009) A novel agricultural waste adsorbent for the removal of cationic dye from aqueous solutions. J Hazard Mater 162:305–311

Ho YS, McKay G (1998) Kinetic models for the sorption of dye from aqueous solution by wood. Process Saf Environ Prot 76:332–340

Huang YH, Huang GH, Chou S, Perng HS (2000) Process for chemically oxidizing wastewater with reduced sludge production. US Patent US6143182 Nov 2000

Jorfi S, Ahmadi MJ, Pourfadakari S, Jaafarzadeh N, Soltani RDC, Akbari H (2017) Adsorption of Cr(VI) by natural clinoptilolite zeolite from aqueous solution: isotherms and kinetics. Pol J Chem Technol 19:106–114

Kamaraj R, Ganesan P, Vasudevan S (2015) Removal of lead from aqueous solutions by electrocoagulation: isotherm, kinetics and thermodynamic studies. Int J Environ Sci Technol 12:683–692

Khazaei M, Nasseri S, Ganjali MR, Khoob M, Nabizadeh R, Medhi AH, Nazmara S, Gholibegloo E (2016) Response surface modeling of lead (II) removal by graphene oxide-Fe_3O_4 nanocomposite using central composite design. J Environ Health Sci Eng 14:1–14

Khuri AI, Mukhopadhyay S (2010) Response surface methodology. WIREs Computational Statistics, vol 2. Wiley, 128–149

Lim S, Lee AYW (2015) Kinetic study on removal of heavy metal ions from aqueous solution by using soil. Environ Sci Pollut Res 22:10144–10158

Malkoc E (2006) Ni(II) removal from aqueous solutions using cone biomass of Thuja oriental. J Hazard Mater B137:899–908

Mohamed Z, Abdelkarim A, Ziat K, Mohamed S (2016) Adsorption of Cu(II) onto natural clay: equilibrium and thermodynamic studies. J Mater Environ Sci 7:566–570

Mohapatra M, Khatum S, Anand S (2009) Adsorption behaviour of Pb(II), Cd(II) and Zn(II) on NALCO plant sand. Indian J Chem Technol 16:291–300

Montgomery DC (2005) Design and analysis of experiment. Wiley, New York

Muthu K, Viruthagiri T (2015) Study on solid based calcium oxide as a heterogeneous catalyst for the production of biodiesel. J Adv Chem Sci 1:160–163

Na P, Jia X, Yuan B, Li Y, Na J, Chen Y, Wang L (2010) Arsenic adsorption on Ti-pillared montmorillonite. J Chem Technol Biotechnol 85:708–714

Nguyen TC, Loganathan P, Nguyen TV, Vigneswaran S, Kandasamy J, Naidu R (2015) Simultaneous adsorption of Cd, Cr, Cu, Pb and Zn by an iron-coated Australian zeolite in batch and fixed-bed column studies. Chem Eng J 2:1–36

Obeng DP, Morrell S, Napier-Munn TJ (2005) Application of central composite rotatable design to modeling the effect of some operating variables on the performance of the three –product cyclone. Int J Miner Process 76:181–192

Olutoye MA, Hameed BH (2013) A highly active clay-based catalyst for the synthesis of fatty acid methyl ester from waste cooking palm oil. Appl Catal A Gen 450:57–62

Rai MK, Shukla MM, Doris KL, Shukla A, Rai BN (2016) Removal of hexavalent chromium Cr(VI) using activated carbon prepared from mango kernel activated with H_3PO_4. Resourc Effic Technol 2:S63–S70

Ridha MJ, Ahmed AS, Raoof NN (2017) Investigation of the thermodynamic, kinetic and equilibrium parameters of batch biosorption of Pb(II), Cu(II) and Ni(II) from aqueous phase using low cost biosorbent. Al-Nahrain J Eng Sci (NJES) 201:298–310

Selvaraj K, Manonmani S, Pattabhi S (2003) Removal of hexavalent chromium using distillery sludge. Bioresour Technol 89:207–211

Sharma YC, Singh B, Korstad J (2010) Application of an efficient non-conventional heterogeneous catalyst for biodiesel synthesis from *Pongamia pinnata* oil. Energy Fuel 24:3223–3231

Sumathi KMS, Mahimairaja S, Naidu R (2005) Use of low-cost biological waste and vermiculite for removal of chromium from tannery effluent. Bioresour Technol 96:309–316

Tan IAW, Ahmed AL, Hameed BH (2008) Preparation of activated carbon from coconut husk: optimization study on removal of 2, 4, 6-trichlorophenol using response surface methodology. J Hazard Mater 153:709–717

Tan YH, Abdullah MO, Hipolito CN, Taufiq-Yap YH (2015) Waste ostrich and chicken-eggshells as heterogeneous base catalyst for biodiesel production from used cooking oil: catalyst characterization and biodiesel yield performance. Appl Energy 2:1–13

Vasudevan S, Lakshmi J (2012) Electrochemical removal of boron from water: adsorption and thermodynamic studies. Can J Chem Eng 90:1017–1026

Vasudevan S, Lakshmi J, Sozhan G (2011) Studies on the Al-Zn-In-alloy as anode material for the removal of chromium from drinking water in electrocoagulation process. Desalination 275:260–268

Vasudevan S, Lakshmi J, Kamaraj R, Sozhan G (2013) A critical study on the removal of copper by an electrochemically assisted coagulation: equilibrium, kinetics, and thermodynamics. Asia Pac J Chem Eng 8:162–171

Wang LH, Lin CI (2008) Adsorption of lead ion from aqueous solution using rice hull ash. Ind Eng Chem Res 47:4891–4897

Yu LJ, Shukla SS, Dorris KL, Shukla A, Margrave JL (2003) Adsorption of chromium from aqueous solutions by maple sawdust. J Hazard Mater 100:53–63

Yuan P, Fan M, Yang D (2009) Montmorillonite-supported magnetite nanoparticles for the removal of hexavalent chromium [Cr(VI)] from aqueous solutions. J Hazard Mater 166:821–829

Yusuff AS (2017) Preparation and characterization of composite anthill-chicken eggshell adsorbent: optimization study on heavy metals adsorption using response surface methodology. J Environ Sci Technol 10:120–130

Yusuff AS, Olateju II, Ekanem SE (2017) Equilibrium, kinetic and thermodynamic studies of the adsorption of heavy metals from aqueous solution by thermally treated quail eggshell. J Environ Sci Technol 10:246–257